

# Thermoresponsive Magnetic Hydrogels as Theranostic Nanoconstructs

Manish K. Jaiswal,<sup>†,‡</sup> Mrinmoy De,<sup>‡,§</sup> Stanley S. Chou,<sup>‡,§</sup> Shaleen Vasavada,<sup>‡</sup> Reiner Bleher,<sup>‡</sup> Pottumarthi V. Prasad,<sup>||</sup> Dhirendra Bahadur,<sup>\*,†,⊥</sup> and Vinayak P. Dravid<sup>\*,‡,§</sup>

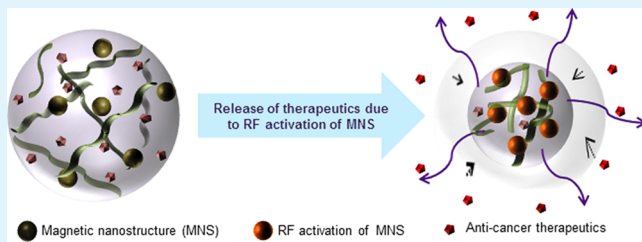
<sup>†</sup>Metallurgical Engineering & Materials science and <sup>‡</sup>Centre for Research in Nanotechnology and Science, Indian Institute of Technology Bombay, Mumbai, MH 400076, India

<sup>§</sup>Department of Materials Science & Engineering and <sup>§</sup>International Institute of Nanotechnology, Northwestern University Evanston, Illinois 60208, United States

<sup>||</sup>Department of Radiology, Northshore University Healthcare, Evanston, Illinois 60201, United States

## Supporting Information

**ABSTRACT:** We report the development of thermoresponsive magnetic hydrogels based on poly(*N*-isopropylacrylamide) encapsulation of  $\text{Fe}_3\text{O}_4$  magnetic nanostructures (MNS). In particular, we examined the effects of hydrogels encapsulated with poly-ethylene glycol (PEG) and polyhedral oligomeric silsesquioxane (POSS) surface modified  $\text{Fe}_3\text{O}_4$  MNS on magnetic resonance (MR)  $T_2$  (transverse spin relaxation) contrast enhancement and associated delivery efficacy of absorbed therapeutic cargo. The microstructural characterization reveal the regular spherical shape and size ( $\sim 200$  nm) of the hydrogels with elevated hydrophilic to hydrophobic transition temperature ( $\sim 40$  °C) characterized by LCST (lower critical solution temperature) due to the presence of encapsulated MNS. The hydrogel-MNS (HGMNS) system encapsulated with PEG functionalized  $\text{Fe}_3\text{O}_4$  of 12 nm size (HGMNS-PEG-12) exhibited relaxivity rate ( $r_2$ ) of  $173 \text{ mM}^{-1}\text{s}^{-1}$  compared to  $129 \text{ mM}^{-1}\text{s}^{-1}$  obtained for hydrogel-MNS system encapsulated with POSS functionalized  $\text{Fe}_3\text{O}_4$  (HGMNS-POSS-12) of the same size. Further studies with HGMNS-PEG-12 with absorbed drug doxorubicin (DOX) reveals approximately two-fold enhance in release during 1 h RF (radio-frequency) field exposure followed by 24 h incubation at 37 °C. Quantitatively, it is  $2.1 \mu\text{g mg}^{-1}$  (DOX/HGMNS) DOX release with RF exposure while only  $0.9 \mu\text{g mg}^{-1}$  release without RF exposure for the same period of incubation. Such enhanced release of therapeutic cargo is attributed to micro-environmental heating in the surroundings of MNS as well as magneto-mechanical vibrations under high frequency RF inside hydrogels. Similarly, RF-induced in vitro localized drug delivery studies with HeLa cell lines for HGMNS-PEG-12 resulted in more than 80% cell death with RF field exposures for 1 h. We therefore believe that magnetic hydrogel system has in vivo theranostic potential given high MR contrast enhancement from encapsulated MNS and RF-induced localized therapeutic delivery in one nanoconstruct.



**KEYWORDS:** *poly(*N*-isopropylacrylamide), magneto-thermo responsive polymers, MR active hydrogels, cellular uptake of hydrogels, PEG-functionalized  $\text{Fe}_3\text{O}_4$ , POSS-functionalized  $\text{Fe}_3\text{O}_4$*

## 1. INTRODUCTION

Thermoresponsive hydrogels are often termed as “soft smart materials”<sup>1</sup> because of their ability to transition between hydrophilic and hydrophobic states as a function of temperature. At temperatures above the material’s intrinsic lower critical solution temperature (LCST), the hydrogels expel its water content to form globules. This occurs because hydrophobic constituents of the polymers forming the hydrogel become active with temperature, resulting in thermally induced conformational changes.<sup>2</sup> The process of hydrophilic to hydrophobic transition at LCST is reversible, which enables its usage in carrying and releasing aqueous soluble therapeutics as controlled drug delivery system.<sup>3,4</sup> In addition to the temperature sensitivity, by virtue of its soft porous nature, hydrogels may be made sensitive to mechanical oscillations/

vibrations like those generated from high-frequency RF field, which can rupture and widen the mesh structure if incorporated with magnetic nanostructures (MNS).<sup>5</sup> Thus, the added advantage of such magneto-thermo responsive hydrogels is that the loaded therapeutics could be released due to synergistic effects of both temperature<sup>6–8</sup> and magnetic vibrations under the applied RF field<sup>5</sup> (schematic shown in Figure 1). Apart from this the role of MNS as MR (magnetic resonance) contrast agent,<sup>9</sup> raising the LCST of hydrogels above physiological conditions are also well-reported.<sup>10,11</sup>

**Received:** July 30, 2013

**Accepted:** April 9, 2014

**Published:** April 9, 2014

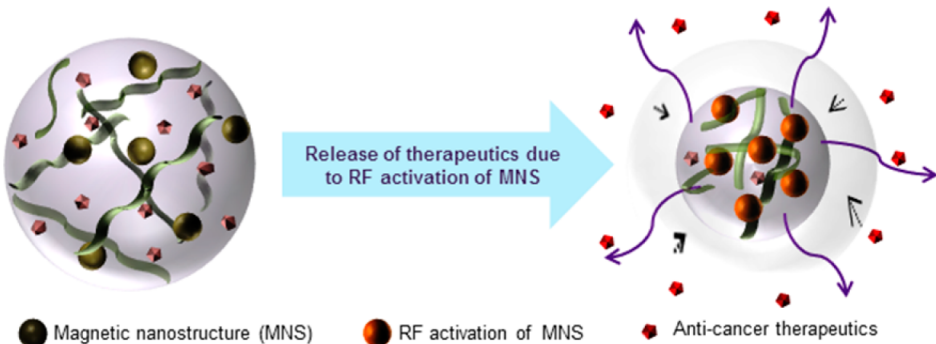


**Figure 1.** Schematic illustration showing thermoresponsive hydrogel's structural collapse with RF (thermal) activation of MNS, thereby triggering the release of therapeutic cargo.

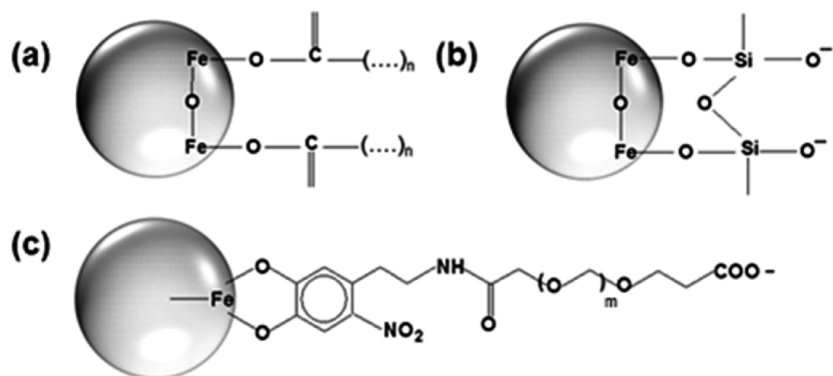


**Figure 2.** Illustration of chemical stabilization of Fe<sub>3</sub>O<sub>4</sub>-based MNS. (a) Oleic acid functionalization onto the MNS surface, which provides MNS stability in organic solvent due to the interaction of the elongated long-chain aliphatic group. (b, c) POSS and nitro-dopamine PEG-diacid-functionalized MNS, which offer a high degree of aqueous stability due to unsaturated carbonyl and carboxylic groups.

Poly(*N*-isopropylacrylamide), (poly(NIPAAm)) is one of the most widely used thermoresponsive polymers due to the proximity of its LCST  $\sim$  30–32 °C to physiological temperature.<sup>12–15</sup> It has thus been used in a wide range of biomedical applications such as drug delivery carriers,<sup>16,17</sup> tissue engineering scaffolds,<sup>18</sup> cell growth/separation supports,<sup>19</sup> fluorescence thermo-sensing,<sup>20</sup> DNA sensing<sup>21</sup> and water remediation through organic dyes removal<sup>22</sup> among others.<sup>23</sup> Here we demonstrate tailoring of the MNS surface via different ligands conjugation; poly-ethylene glycol (PEG) and polyhedral oligomeric silsesquioxane (POSS) using reported methods,<sup>24,25</sup> to enable uniform encapsulation throughout the NIPAAm (*N*-isopropylacrylamide) cross-linking process. The selection of PEG is quite evident as it provides enhanced aqueous stability and prolonged blood circulation to the MNS.<sup>24,26,27</sup> POSS on the other hand has a tetrahedral cage-like structure with eight oxygen ions at the corners out of which four interact with surface Fe atoms of Fe<sub>3</sub>O<sub>4</sub> MNS and other four interact with water molecules and thus expected to provide a high degree of colloidal stability over wide range of pH and ionic strengths.<sup>25</sup>

We report the development of spherically shaped nanoscale hybrid hydrogels (~200 nm) with poly(NIPAAm) and Fe<sub>3</sub>O<sub>4</sub> MNS (9 or 12 nm) which demonstrate multimodal imaging, remote RF-triggered release of therapeutic cargo and resulting cell death for cancer theranostics (simultaneous therapy and diagnostic application). In particular, we compare the drug release behavior of anti-cancer drug doxorubicin (DOX) under two different conditions: (1) temperature as stimulant for release in a water bath set at 42  $\pm$  2 °C, and (2) RF field as an external stimulant for cargo release involving both magnetic

heating and magneto-mechanical vibrations. We further investigated its cell viability using human cervical carcinoma cell lines (HeLa) through RF-triggered release of DOX. Lastly, we report the cellular uptake of these thermoresponsive magnetic hydrogels through STEM (scanning transmission electron microscope) observations; a first direct confirmation of such cellular transfection.

## 2. EXPERIMENTAL SECTION

**2.1. Materials.** *N*-Isopropylacrylamide (NIPAAm, 97 %), ammonium persulfate (APS, 98%), sodium metabisulfite (SBS, 99%), ferric chloride hexahydrate (FeCl<sub>3</sub>·6H<sub>2</sub>O,  $\geq$  98%), sodium oleate ( $\geq$  99%), doxorubicin.HCl (DOX, HPLC grade), fluorescein (95%), crosslinker *N,N'*-methylene-bis-acrylamide (MBAAm, 99%), dopamine hydrochloride (dopamine, 98%), poly-ethylene glycol (PEG, mol. wt. 310), PSS hydrate octakis(tetramethylammonium) (POSS), *N,N'*-dicyclohexylcarbodiimide (DCC, 99%), *N*-hydroxysuccinimide (NHS, 98%), solvents ethanol, dimethyl sulfoxide (DMSO), chloroform, and 1-octadecane were all purchased from Sigma-Aldrich, USA. All chemicals were directly used without further purification. Megaohm water (18.2 MΩ·cm) was used for all experiments.

**2.2. Methods.** *Magnetic Nanostructure (MNS) Synthesis.* MNS were synthesized using previously reported methods.<sup>28</sup> In brief, 10.8 g of FeCl<sub>3</sub>·6H<sub>2</sub>O and 36.5 g of sodium oleate dissolved in a mixture of 80 mL of ethanol, 140 mL of hexane, and 60 mL of water was refluxed at 70 °C for 4 h to obtain the iron-oleate complex. 5.815 g (ca.) of the obtained iron-oleate complex was dissolved in 40 mL of 1-octadecane and 1.04 mL of oleic acid and the mixture was equilibrated at 25 °C for 10 min and subsequently raised to 318 °C at a ramp rate of 3.3 °C min<sup>-1</sup>. The system was refluxed for next 10 or 15 min to produce hydrophobic crystals of Fe<sub>3</sub>O<sub>4</sub> with 9 or 12 nm diameters.

**Ligand Replacement by PEG and POSS.** Hydrophobic  $\text{Fe}_3\text{O}_4$  was transferred into water by use of PEG and POSS ligands (schematic illustration shown in Figure 2). PEG-dicarboxylate functionalization<sup>24</sup> was achieved by mixing 80 mg of HOOC-PEG-COOH dissolved in 30 mL of chloroform and 55.8 mg of nitro-dopamine (which is prepared from dopamine according to the reported method (see the Supporting Information)) dissolved in 15 mL of DMSO in single-neck flask and sonicated. Subsequently, 49.5 mg of DCC was dissolved and thereafter 100 mg of  $\text{NaHCO}_3$  and 27 mg of NHS were added to it. The entire mixture was purged under  $\text{N}_2$  for 30 s before putting on vigorous stirring for 24 h. About 200  $\mu\text{L}$  of hydrophobic- $\text{Fe}_3\text{O}_4$  MNS (20 mg  $\text{mL}^{-1}$ ) in hexane precipitated out in the mixture of ethyl acetate, and methanol (80:20 v/v) was mixed with this solution and sonicated for 48 h to produce hydrophilic MNS.

For POSS functionalization,<sup>25</sup> 200 mg of POSS dissolved in 2 mL of water was mixed with 5 mg  $\text{mL}^{-1}$  oleic acid- $\text{Fe}_3\text{O}_4$  in hexane, followed by stirring the solution. The obtained PEG and POSS functionalized  $\text{Fe}_3\text{O}_4$  MNS were further dialyzed against ultrapure water for 6 h (molecular wt. cut-off  $\sim$ 10 kDa) and then collected for synthesis of HGMNs.

**Synthesis of Magnetic Hydrogels:  $\text{Fe}_3\text{O}_4$  MNS Embedded in Hydrogels.** Encapsulation of MNS in poly(NIPAAm) hydrogels was achieved by mixing varying concentrations of MNS (100, 200, and 500 Fe ppm) with NIPAAm monomers in water (361.6 mg, 80 mL). Free radical chain polymerization was initiated with APS addition (9.12 mg, 8 mL water) and catalyzed by SBS (2 mg, 8 mL of water). Reactions were carried in a 250 mL 4-neck flask with vigorous stirring for 5 h under a  $\text{N}_2$  atmosphere. The products were dialyzed against ultrapure water for 5 days. Iron contents in the resultant product were measured using ion coupled plasma atomic emission spectroscopy (ICP-AES).

**2.3. Drug Delivery and Cell Cytotoxicity Studies.** First, fluorescein was chosen to investigate the RF field activated release by fluorescence response and Dox was used to study the cell death behavior via magnetic hydrogel. The fluorescence data were recorded using fluorometric micro-plate reader excited at 490 nm. In brief, for encapsulation 4 mg of sample plus 100 (or 50)  $\mu\text{g}$  of DOX (or fluorescein) was properly dispersed/sonicated in 500  $\mu\text{L}$  of water in microcentrifuge tubes in triplicates and maintained at 4 °C for overnight to let the hydrogels swell and entrap the cargo. The obtained sample loaded with cargo was centrifuged and washed thrice with chilled water to separate out the unloaded cargo. The encapsulation/entrapment efficiency (EE), feed weight ratio (FWR), and loading content (LC) were estimated using the formula below:<sup>29</sup>

$$\text{encapsulation efficiency (EE)} = \frac{\text{weight of encapsulated cargo}}{\text{weight of feed cargo}} \times 100 \quad (1)$$

$$\text{feed weight ratio (FWR)} = \frac{\text{weight of feed cargo}}{\text{weight of host sample}} \times 100 \quad (2)$$

$$\text{loading content (LC)} = \frac{\text{weight of encapsulated cargo}}{\text{weight of host sample}} \times 100 \quad (3)$$

For triggered release sample loaded with drug was homogeneously mixed in 3 mL of water and trifurcated into three different microcentrifuge tubes with 1 mL in each. The three tubes were further subjected to water-bath (tube 1, 42 ± 2 °C), RF field (tube 2, 5 kW, 230 kHz, 180 Oe), and control (tube 3, no RF) for 1 h simultaneously. Subsequently all the tubes were centrifuged and supernatant which contains released drug was collected for estimation. The obtained results for release are discussed in the Supporting Information.

Further based on the previous results, the HGMNS-PEG-12 sample was chosen to demonstrate the cell death efficacy of the hydrogels. To ascertain the dosage for cell treatment, we carried out a detail drug release study using 4 mg of sample loaded with DOX under various thermal conditions. The sample taken in microcentrifuge tube in 500  $\mu\text{L}$  of water was exposed to RF for different durations (1, 2, and 3 h) and kept inside incubator at 37 °C for different time intervals; 24 and

48 h thereafter. The released amounts of DOX were obtained by using fluorescence intensity measurements.

To demonstrate the therapeutic efficacy to cancer cells, the RF-induced cargo release experiments were performed using HGMNS-PEG-12 on human cervical carcinoma (HeLa) cell lines. In brief, 15 000 cells were taken in 5 equiv in 500  $\mu\text{L}$  of media volume in microcentrifuge tubes. The tubes were labeled as (1) control, (2) HGMNS-12, (3) HGMNS-12 + DOX, (4) HGMNS-12 + DOX + RF, (5) control + RF, respectively. Whereas tube 2 was incubated with 4 mg of sample only, tubes 3 and 4 were incubated with sample loaded with DOX and tube 4 in addition was exposed to RF for 1 h. All the tubes were further plated in 96-well plate by 100  $\mu\text{L}$  in each well sequentially and maintained for 6 h at 37 °C in the incubator. Standard protocol for MTS assay was followed to determine the number of live cells.

**2.4. Imaging of Hydrogel's Cellular Uptake.** The imaging of cellular uptake of hydrogels was carried out using STEM (scanning transmission electron microscopy). The sample preparation protocol, in brief, is as follows; HeLa cells grown at a confluence of 80% were incubated with 30 mg HGMNS-PEG-12 for 24 h in T-75 flasks. Thereafter, the cells were trypsinized and washed with PBS (Dulbecco's phosphate-buffered saline, Cellgro Mediatech, Inc., VA) before centrifugation at 400g for 5 min. The supernatant was aspirated and 1.5 mL of 2.5% glutaraldehyde (25% aqueous stock solution), 2% formaldehyde (16% aqueous stock solution) (EMS, Electron Microscopy Sciences) in PBS, pH 7.4, were added. After fixation overnight at 4 °C, the samples were rinsed in PBS and in double-distilled water (ddH<sub>2</sub>O) for 15 min each and post fixed in aqueous 2% Osmium tetroxide (EMS) for 1 h. After two rinses in double-distilled water for 15 min each, the specimens were dehydrated sequentially in 25, 50, 75, and 90% ethanol for 20 min each, and two times for 10 min each in 100 % ethanol. After infiltration with a 1:1 mixture of Spurr resin (EMS) and ethanol for 3 h, the samples were infiltrated overnight in pure resin. For polymerization, the samples were transferred into fresh resin in flat embedding molds and polymerized at 60 °C for 48 h. The blocks were sectioned using a diamond knife (Diatome) with an ultramicrotome (UC7, Leica) at a nominal thickness of 70 nm, and the sections were collected on 200 mesh nickel grids dried and observed in a STEM (HD2300-A, Hitachi) with an acceleration voltage of 80 kV.

The iron uptake of HeLa cell lines for the sample HGMNS-PEG-12 was estimated using ICP-MS (inductive coupled plasma-mass spectroscopy). In a typical experiment 24-well plate was harvested with 40 000 cells in each well. After 24 h the cells were properly washed with DPBS (de-ionized phosphate buffer saline) and incubated with samples in amounts of 4, 8, and 16 mg in triplicates and maintained at 37 °C for 24 h under 5 % CO<sub>2</sub> humidified environment along with control. The cells were further washed with DPBS and trypsinized with 200  $\mu\text{L}$  of trypsin and 200  $\mu\text{L}$  of trypsin inhibitor. The cells were counted once again to obtain an accurate iron per cell count. The samples were then collected in 15 mL of falcon tubes, which were further analyzed for iron estimation using ICP-MS (inductively coupled plasma-mass spectroscopy).

### 3. MATERIALS CHARACTERIZATIONS

The synthesized samples, both MNS and hydrogels, were characterized for their structural, microstructural, and physical properties. X-ray diffraction, Fourier transform infra-red (FT-IR), and X-ray photoelectron spectra (XPS) analysis were carried out to confirm the formation of magnetite phase and functionalization of coating molecules over the MNS surfaces, respectively. <sup>13</sup>C-solid state NMR of synthesized hydrogels (HG) was carried out to confirm the polymerization of NIPAAm. Transmission electron microscopy (TEM) to confirm the monodisperse formation of MNS while scanning transmission electron microscopy (STEM), scanning electron microscopy (SEM) and atomic force microscopy (AFM) to confirm the shape and size of hydrogels were carried out. To determine the LCST of the hydrogel composite samples change

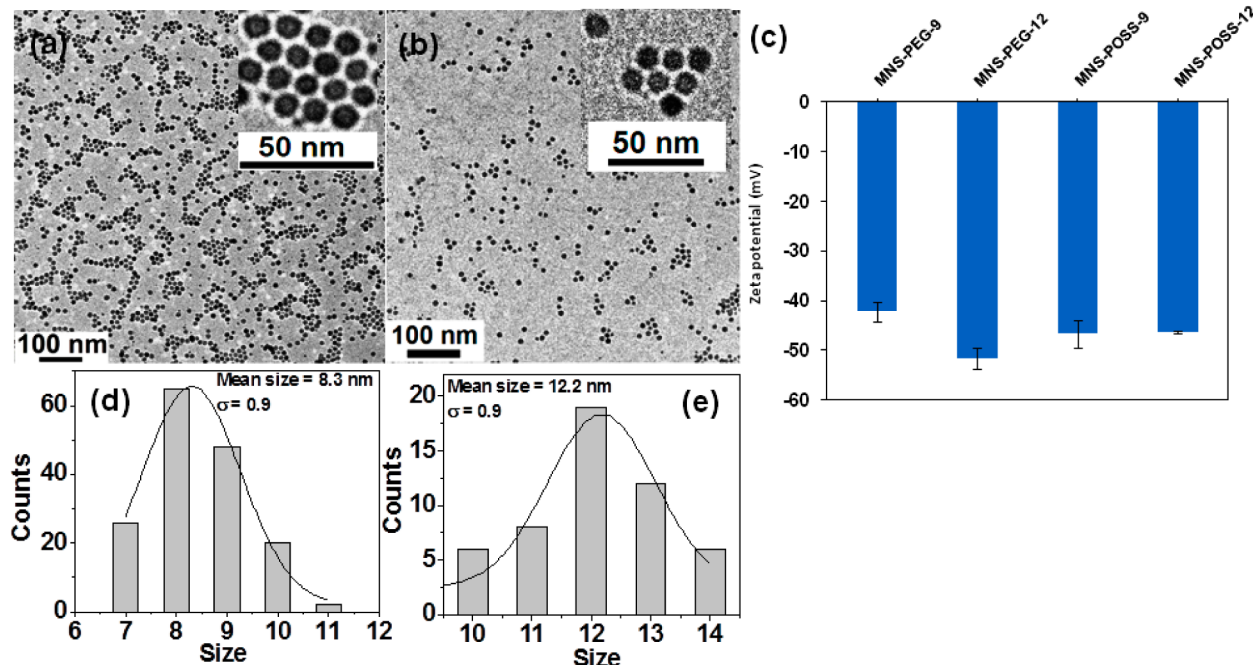


**Figure 3.** TEM images of  $\text{Fe}_3\text{O}_4$  MNS (a) 9 nm and (b) 12 nm; (c) zeta potential of MNS functionalized with PEG and POSS; (d, e) size-distribution histograms of 9 and 12 nm MNS, respectively.

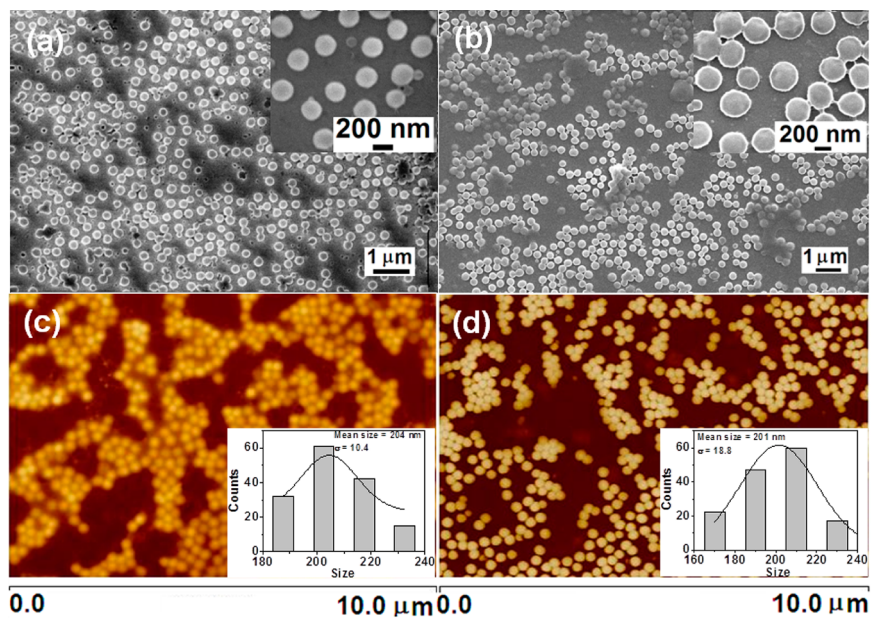


**Figure 4.** Representative (a, b) SEM and (c, d) AFM images of poly(NIPAAm)-based hydrogels revealing its spherical shape and size (200 nm): (a, c) hydrogels without MNS, (b, d) hydrogels embedded with MNS, confirming that the entrapment of  $\text{Fe}_3\text{O}_4$  nanocrystals does not affect the hydrogels morphology. The inset histograms present the size-distribution of respective samples. The mean sizes are (c)  $204 \pm 10$  and (d)  $201 \pm 18$  nm.

in specific heat ( $C_p$ ) versus temperature was recorded in the range of 25–60 °C using reported protocol.<sup>12</sup> For sample preparation, a small amount of the aqueous sample was kept at 4 °C for overnight to entrap water as much as it can. Thereafter it was centrifuged to decant excess water and the obtained slurry was subjected to differential scanning calorimetry (DSC) at constant pressure under inert conditions. Further the hydrogel samples encapsulated with MNS were investigated for their  $T_2$  (transverse spin relaxation)-weighted contrasts enhance properties using commercial MR relaxometry. The

pre-equilibrated aqueous dispersions of serially diluted hydrogel sample solutions; HGMNS-PEG-12, HGMNS-PEG-9\*, HGMNS-POSS-12, HGMNS-POSS-9\* at 37 °C were subjected to MR relaxometer (3T) to acquire  $T_2$  values for different Fe concentrations. The relaxivity values ( $r_2$ ) were calculated from the slope of  $1/T_2$  versus Fe concentration for each sample. Further, the room-temperature  $T_2$ -weighted phantom images of the aqueous dispersions of the same samples were acquired under clinical MRI scanner (GE healthcare, USA) with multiple spin echo sequence, 8

(repetition time TR/Echo time TE = 1290 ms/9.9, 19.8, 29.7, 39.6, 49.5, 59.4, 69.3, 79.2 ms), field of view FOV 160 mm, matrix size 256 × 256, and slice thickness = 3 mm.

#### 4. RESULTS AND DISCUSSION

The size, shape and monodispersity of the desired  $\text{Fe}_3\text{O}_4$  nanostructures were confirmed by TEM prior to PEG/POSS functionalization (Figure 3a, b). The zeta-potential (Figure 3c) after functionalization was found to be in the range of  $-40 \text{ mV}$ , consistent with their colloidal stability in water.

The surface morphology and topography of hydrogels were further characterized using SEM and AFM. Figure 4 shows the representative SEM and AFM images of HG (a, c) and HGMNS (b, d) samples on silica substrate. Spherical shape and monodispersed size distribution with the typical size of  $\sim 200 \text{ nm}$  was observed.

The presence of MNS inside hydrogel structures was confirmed under both bright and dark field imaging in TEM and by EDS (energy-dispersive X-ray spectroscopy) analysis. Both the bright and dark field images suggest a dense inorganic core (Figure 5a, b) covered by low contrast organic shadow.

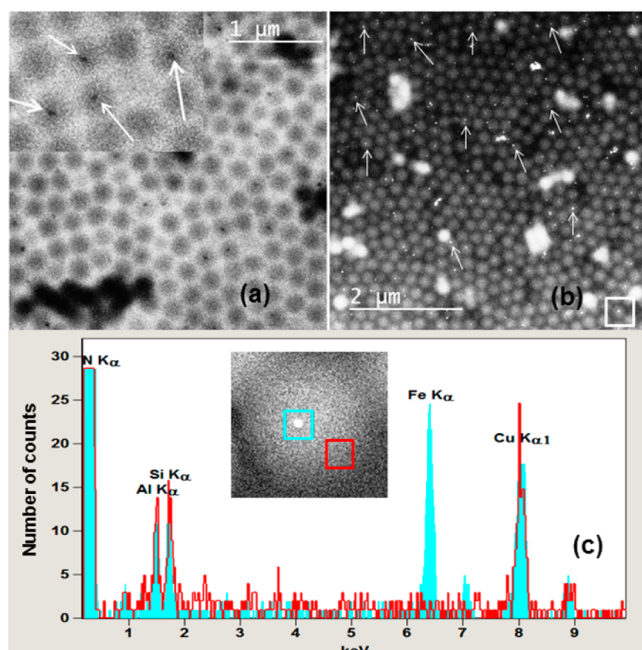


**Figure 5.** Representative TEM micrographs of hydrogels embedded with  $\text{Fe}_3\text{O}_4$  MNS. (a, b) Bright- and dark-field pictures of hydrogels which appear very regular in shape and size where arrows pointing to the MNS. Inset in a is the magnified image of iron oxide as black dots. (c) EDS mapping for iron in the magnified version of HGMNS shown by square box in b. The peaks observed in the EDS plot for the selected area colored in blue (containing core particles) and red (neat organic region) confirms the presence of  $\text{Fe}_3\text{O}_4$  embedded into hydrogel.

The iron content inside hydrogels can be explicitly identified using EDS (Figure 5c). Further structural characterization data on X-ray diffraction of MNS (Figure S1a in the Supporting Information) along with Fourier transform infra-red (FT-IR) spectroscopy (see Figure S1b in the Supporting Information) and X-ray photoelectron spectroscopy (XPS) of coated MNS (see Figure S2 in the Supporting Information) to confirm the coating of MNS with PEG and POSS are presented in the

Supporting Information. Figure S3 and Figure S4 show the nuclear magnetic resonance (NMR) spectra to confirm the polymerization of NIPAAm and the iron quantification through ICP-AES along with magnetization measurements of hydrogels-MNS samples using SQUID (superconducting quantum interference device) in the Supporting Information.

Figure 6 shows the LCST determination of all the four HGMNS samples using DSC thermogram. The peak represents

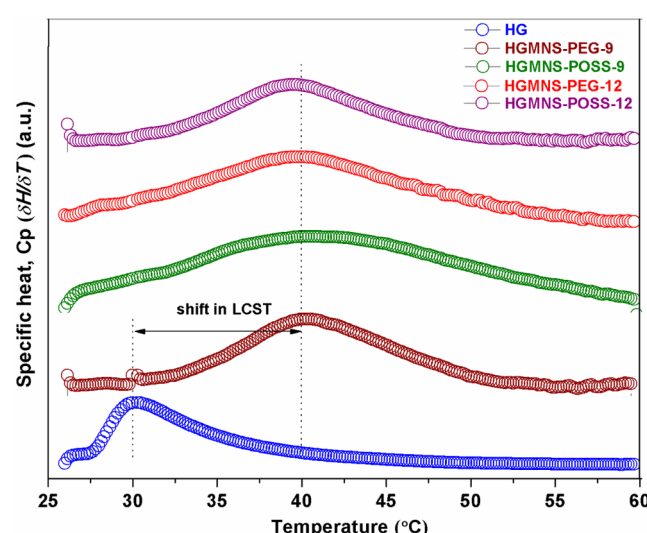


**Figure 6.** Differential scanning calorimetric (DSC) thermograms of hydrogel-MNS samples along with base hydrogel (HG). The presence of  $\text{Fe}_3\text{O}_4$  MNS causes upward shifting in LCST of HG by about  $10 \text{ }^\circ\text{C}$  as indicated by the peak positions, with little broader transition.

the endothermic change in the system as the temperature crosses LCST. The LCST of poly(NIPAAm)-HG is found to be approximately  $30 \text{ }^\circ\text{C}$ . However, for HGMNS samples, relatively a broad transition is observed with a maximum around  $40 \text{ }^\circ\text{C}$ . The observed upward shifting in LCST of about  $10 \text{ }^\circ\text{C}$  due to presence of MNS into hydrogels is consistent with the earlier reports.<sup>10</sup>

Because the LCST of hydrogels is the result of competition between hydrophilic and hydrophobic constituents of the hydrogels, it is expected that due to the introduction of aqueous stabilized MNS, there should be upward shifting in the LCST of HGMNS because of the hydrophilic nature of PEG- and POSS-coated  $\text{Fe}_3\text{O}_4$  MNS. It may also be noted that the cross-linking of PEG with NIPAAm has already been reported to have raised the LCST of polymeric hydrogels and we believe the aqueous stabilized POSS nanostructures would equally cause shift in it if incorporated within hydrogels because of their hydrophilic character.

Similar studies carried out with poly(vinyl alcohol) (PVA) gels incorporated with  $\text{Fe}_3\text{O}_4$  MNS resulted into nanostructures providing “barrier to heat” to the polymer segments.<sup>30</sup> It is postulated that the adhesive interaction between nanostructures and polymer matrix restrict the segments mobility and thus leads to greater degree of thermal stability. This phenomenon of the rise in transition temperature finds a parallel in the polymer–nanostructure filler effect, where “hard” silica nanospheres act as obstacles to the inter-diffusion of “soft” polymeric segments of poly(butyl methacrylate) and thereby alter the diffusion rate of the polymer and raises the glass transition.<sup>31</sup>

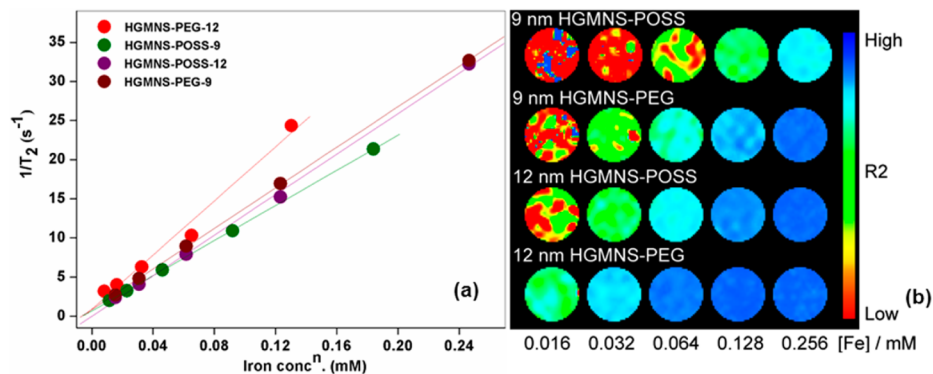


**Figure 7.** MR contrast characteristics of hydrogel-MNS samples. (a) Relaxivity rate ( $r_2$ ) measurements of HGMNS embedded with PEG and POSS functionalized MNS (9 and 12 nm). The  $r_2$  is the slope of the straight-fit line drawn for  $1/T_2$  vs. iron concentrations of the corresponding sample. (b)  $T_2$ -weighted phantom color images at five serially diluted iron concentrations of the same samples corroborating the  $r_2$  data.

$\text{Fe}_3\text{O}_4$  plays an important role in diagnostic imaging of cancer because of its  $T_2$  MR contrast enhancement characteristic when localized at the lesion site. The MR contrast enhancement can be understood in terms of shortening of spin–spin relaxation time characterized by  $T_2$ . Figure 7a shows the plot of  $1/T_2$  versus iron concentration plot of four major HGMNS samples with highest iron content (500 ppm of Fe). The slope of the straight-fit line yields the  $r_2$  value for the corresponding plot. The  $r_2$  values are found to be higher for hydrogels embedded with  $\text{PEG}-\text{Fe}_3\text{O}_4$  than that of  $\text{POSS}-\text{Fe}_3\text{O}_4$  for the same size of MNS. Quantitatively, it is  $173 \text{ mM}^{-1} \text{ s}^{-1}$  for HGMNS-PEG-12 against  $129 \text{ mM}^{-1} \text{ s}^{-1}$  for HGMNS-POSS-12, whereas these values are  $129$  and  $112 \text{ mM}^{-1} \text{ s}^{-1}$  respectively for 9 nm size. These differences further suggest the formation of large localized aqueous layer around MNS surface in case of PEG than that in POSS leading it to shorter spin–spin relaxation time ( $T_2$ ). Apart from this, for larger size, 12 nm, the  $r_2$  values are higher than that of smaller size, 9 nm, MNS for the functionalization, which can be attributed to the more pronounced spin-canting effect in smaller-sized MNS.<sup>32</sup>

Here, it is imperative to bring the concept propounded and studied by Vuong and Pothayee et al.<sup>33,34</sup> to empirically estimate the  $r_2$  of the MNS which has square dependency with size ( $d$ ) divided by internal volume fraction ( $\Phi_{\text{intra}}$ ) of hydrated MNS. The ratios of relaxivities ( $r_2$ ) for hydrogels embedded with PEG and POSS functionalized MNS of the sizes 12 and 9 nm are calculated to be approx. 1.34 and 1.15, respectively. When these values are compared with the empirically calculated ratio for the squares of the diameter of the MNS (excluding the factor of  $\Phi_{\text{intra}}$ ), which is approx. 1.77, these are found to be a bit smaller. The differences can be attributed to the several experimental parameters like spacing in embedded MNS inside hydrogels, the variation in  $\Phi_{\text{intra}}$ , and variation in water diffusion coefficient inside hydrogels.<sup>34</sup>

Figure 7b is the room temperature  $T_2$ -weighted phantom color images for serially diluted iron concentrations corroborating the data obtained for relaxivity of the corresponding samples. The rise in the color inhomogeneity from higher to lower Fe concentration can be ascribed to the dominant noise level in the MR contrast images.

Some recent reports on MR relaxivities measurements for MNS-based systems are worth to be discussed here. Recently, Barick et al.<sup>35</sup> synthesized carboxyl-functionalized MNS of  $6 (\pm 0.5)$  nm size and noted the  $r_2$  values of approximately  $197 \text{ mM}^{-1} \text{ s}^{-1}$  studied under for the same field parameters. In contrast, the obtained difference in  $r_2$  value obtained for MNS

when embedded in hydrogel (e.g., HGMNS-PEG-12,  $\sim 173 \text{ mM}^{-1} \text{ s}^{-1}$ ) can be attributed to the hydrogel encapsulation of MNS, which hinders their extended aqueous interaction in the solution. Furthermore, on a comparative note, Balasubramanian and co-workers<sup>36</sup> reported the poly(NIPAAm)-coated  $\text{Fe}_3\text{O}_4$  MNS for their temperature-dependent  $T_2$  relaxation behavior. However, the system does not serve the purpose of carrying a therapeutic with it and to delivering it upon RF stimulation at the site of interest. More recently, Zhu et al.<sup>37</sup> designed a thermoresponsive magnetic/optical imaging probe with poly(styrene-NIPAAm) core–shell nanoparticles encasing  $\text{Eu}^{3+}$  and  $\text{Fe}_3\text{O}_4$  MNS. The animal experiments carried out on rats exhibited significantly high transverse relaxivity values of the system, which reduced the liver and spleen  $T_2$ -weighted signals by about 85%. Furthermore, the observed  $r_2$  values (approx.  $173 \text{ mM}^{-1} \text{ s}^{-1}$ ) for HGMNS-PEG-12 in the present study is quite comparable to the previously reported values for  $\text{Fe}_3\text{O}_4$ -based systems and appear suitable for practical applications.

The samples were further investigated for their drug loading and release efficacy through RF activation of embedded MNS, which may stimulate triggered behavior and hence release the loaded therapeutics. The cargo was encapsulated and delivered from HGMNS-PEG-12 under RF, water-bath, and without RF simultaneously. After encapsulation of cargo, the values of EE, FWR, and LC were calculated for DOX and fluorescein using the eqs 1, 2, and 3, respectively described in section 2.3.

For DOX these values were calculated to be 25% or  $6 \mu\text{g mg}^{-1}$  or  $3.6 \times 10^{-11} \mu\text{g}/\text{hydrogel}$  (EE), 2.5% (FWR), and 0.625 % (LC), whereas for fluorescein, these parameters were 30% or  $3 \mu\text{g mg}^{-1}$  or  $2.2 \times 10^{-11} \mu\text{g}/\text{hydrogel}$  (EE), 1.25% (FWR), and 0.375% (LC), respectively. Clearly the FWR and LC of DOX in hydrogels appeared to be higher than fluorescein. DOX has pKa values of roughly 8.2; because of its amphoteric nature, it gets  $\text{NH}_3^+$  formation in aqueous media due to the protonation of pendent amine group. The net pH of the aqueous suspension of sample with DOX is observed to be approx.  $4.84 \pm 0.02$ , indicating extended interaction of DOX molecules with hydrogels which has negative zeta potentials (approx.  $-9 \text{ mV}$ ), thus facilitating higher loading into hydrogels. Fluorescein on the other hand with pKa value of 6.4 does not exhibit as much solubility because of the presence of carboxyl and hydroxyl groups, which remain partially charged. The net pH of the sample suspension with fluorescein is measured to be  $5.17 \pm 0.08$  indicating a lesser level of pH change leading to comparatively lower FWR and LC values.

The detail results of percent release of DOX and fluorescein from the samples with fluorescence spectral evolution (Figure S6) and further the cumulative DOX release from HGMNS-PEG-12 (Figure S7) are described in the Supporting Information.

To determine the required dose for cell cytotoxicity studies, we exposed 4 mg of sample loaded with DOX to RF for various durations and maintained at 37 °C inside the incubator thereafter to mimic the cellular environment. Figure 8 shows

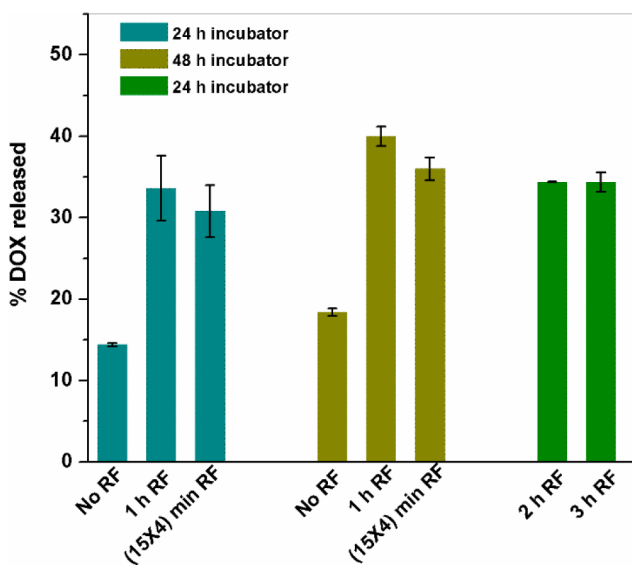


**Figure 8.** DOX release from hydrogels-MNS composite HGMNS-PEG-12 for different time-intervals of RF exposures followed by incubation at 37 °C for the mentioned time period.

the drug release data for HGMNS-PEG-12 when exposed to RF for durations; 1, 2, and 3 h prior to maintaining at 37 °C for 24 or 48 h to mimic the physiological conditions. As can be seen from the plot, 48 h incubation stimulates higher amount of drug release than 24 h incubation at 37 °C for the same duration of field exposure. Furthermore, there is nearly a release of 33% DOX from the sample if exposed to RF for 1 and 24 h incubation at 37 °C as opposed to only 14% if maintained at 37 °C without any prior RF exposures. Furthermore, longer duration (2 or 3 h) of RF exposures as compared to 1 h does not show much enhancement in release percentage indicating RF saturation. Interestingly, the release percentages for four cycles of 15 min RF exposures (total 1 h) each at an interval of 15 min have produced slightly lower drug release than that of 1 h continuous RF exposure. Table 1 displays the details of DOX release from HGMNS-PEG-12 in terms of actual mass.

It should be mentioned here that no temperature rise of the overall solution was noted at macroscopic level when the sample was exposed to RF field for 1 h, possibly because of the low magnetization of the order of ~0.1 emu g<sup>-1</sup> measured in a field of 20 kOe (data shown in the Supporting Information, Figure S4) and/or rapid dissipation of thermal load in the solution. However, a small micro-environmental temperature rise surrounding MNS cannot be ruled out.<sup>38</sup> In a study carried out by Polo et al.<sup>38</sup> when fluorescent-modified poly(NIPAAm) copolymer coated onto Fe<sub>3</sub>O<sub>4</sub> MNS was subjected to RF field, they observed an increased fluorescent intensity instantly without any perceptible macroscopic rise in temperature of the aqueous suspension, suggesting the presence of localized

**Table 1.** Released DOX from HGMNS-PEG-12

S. No.	HGMNS-PEG-12 (4 mg)	released DOX (μg)	% released
1	24 h incubation	3.6 ± 0.05	14.4 ± 0.2
2	48 h incubation	4.6 ± 0.12	18.4 ± 0.48
3	1 h RF + 24 h incubation	8.4 ± 1	33.6 ± 0.4
4	(15 × 4) min RF + 24 h incubation	7.7 ± 0.8	30.8 ± 3.2
5	1 h RF + 48 h incubation	10 ± 0.3	40 ± 1.2
6	(15 × 4) min RF + 48 h incubation	9 ± 0.35	36 ± 1.4
7	2 h RF + 24 h incubation	8.6 ± 0.01	34.4 ± 0.04
8	3 h RF + 24 h incubation	8.6 ± 0.3	34.4 ± 1.2

heating. The synergistic effect of localized heating as well as mechanical vibrations/oscillations of MNS under RF field likely explains the higher percentage release of drug. This is further supported by in vitro cell therapeutic studies discussed next.

Some of the recent research where cargo encapsulation and release has been attempted using composite carriers through localized heating of Fe<sub>3</sub>O<sub>4</sub> NPs are noteworthy here.<sup>39,40</sup> Brule and co-workers<sup>40</sup> synthesized micrometer-size alginate spherical microbeads embedded with NPs for DOX release via RF stimulation. Interestingly, the loading of DOX into microbeads is comparatively low (approx 3.4 μg mg<sup>-1</sup>), whereas the release percentage under 700 kHz and 270 Oe is reasonably high up to 60% because of high RF parameters used. On a comparative note, because of their aqueous content, the hydrogels provide better platform for cargo delivery with considerably smaller size that may facilitate their easy blood circulation.

On the basis of the MR relaxivity rate and drug release data, we selected HGMNS-PEG-12 for cell cytotoxicity studies using HeLa cells under RF field exposure. Images a and b in Figure 9 show the STEM cellular uptake of hydrogel-MNS, whereas panels c and d show the therapeutic efficacy results obtained for HGMNS-PEG-12 and iron uptake estimation using HeLa cell lines. As can be seen in the STEM images, the hydrogel's uptake has taken place after 24 h of incubation. The hydrogels look aggregated and fused which we believe is due to the polymerization temperature ( $\geq 60$  °C) during resin embedding of the sample for imaging. To clarify this, we further carried out STEM imaging of the hydrogel samples dried at 30, 40, 50, 60, and 70 °C for 24 h inside a temperature-controlled incubator. The obtained images confirmed that no distortions or morphological changes appeared up to 50 °C, whereas at 70 °C, they tend to lose their shape and merge altogether. The results are shown in the Supporting Information (Figure S8).

Furthermore, the cell therapeutic effects of HGMNS-PEG-12 shown in Figure 9c indicate that hydrogels are appreciably ( $p \leq 0.005$ ) biocompatible by themselves. However, the viability of cancer cells incubated with DOX-loaded magnetic hydrogels goes down to nearly 70% with respect to control, which further declined significantly ( $p \leq 0.05$ ) to ~20% when exposed to RF for 1 h. Thus, it should be emphasized that the DOX release inside cells under the RF field is primarily responsible for cell death. Here, we believe the local rise in the temperature in the vicinity of MNS<sup>38</sup> inside the hydrogel as well as the magneto-mechanical perturbation<sup>41</sup> together caused by RF field facilitates the enhanced drug release, thereby leading to increased cell death.

The iron uptake estimations of HeLa cells carried out for three different concentrations of HGMNS-PEG-12 along with control using the ICP-MS method are presented in Figure 9d.

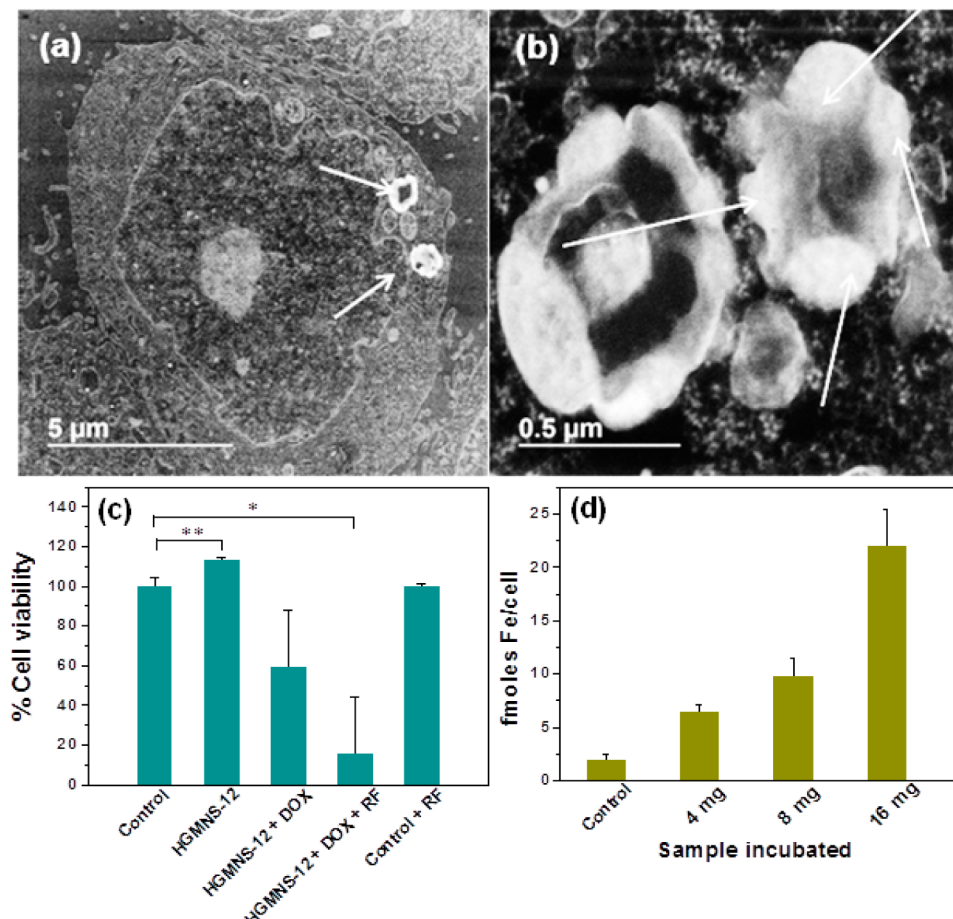


**Figure 9.** STEM images of cellular uptake of magnetic hydrogels. (a, b) Transverse section of cells at (a) low and (b) high magnifications. The hydrogels as indicated by arrows appear fused and aggregated forming a torus ring due to the processing at elevated temperature during cell sample preparation. (c) Percent cell viability of HeLa cell lines treated with HGMNS-PEG-12 and exposed to RF field, along with respective controls. (d) Iron uptake measurements of HeLa cells when sample HGMNS-PEG-12 incubated for 24 h in different concentrations. Results are expressed as mean  $\pm$  s.d. ( $n = 3$ ). \* $p \leq 0.05$  and \*\* $p \leq 0.005$ .

The obtained values expressed in femtomoles indicated the monotonous rise in iron uptake with increased sample concentration from 4, 8, to 16 mg for 24 h incubation. Approximately 22 fmoles iron/cell were obtained for 16 mg of sample incubated into 100 000 cells.

This study was designed to develop a multimodal imaging and therapeutics (theranostic) carrier, which can deliver the anti-cancer agent upon RF activation of magnetic nanostructures with improved efficacy in cancer cell death with low MNS concentration. Because of their thermoresponsive nature, hydrogels provide a soft polymeric mesh for entrapment of MNS as well for therapeutics, which can be released in a controlled fashion by the application of an external high-frequency RF field. Because of the low  $\text{Fe}_3\text{O}_4$  concentration, there is no noticeable macroscopic rise in the hydrogel solution temperature. However, the release profile of DOX suggests that in addition to possible localized temperature rise in close vicinity of MNS, the soft mechanical integrity of the polymeric mesh may be very sensitive to any oscillations/vibrations induced by the RF field and hence influence the drug release behavior significantly. The rapidly oscillating field gradient within the coil may also generate the required mechanical force to rupture the local polymeric mesh, resulting in enhanced release of local therapeutics.

A few studies with this rationale may be worthy of mention. Paoli et al.<sup>5</sup> demonstrated the effect of an oscillating magnetic field (0.3 Hz) on the release behaviour of magnetic collagen gels. They suggested that under the oscillating magnetic field, the magnetic nanostructures vibrate and provide the required force for local release of entrapped cargo. They further concluded that the cell death and the release behavior are mainly due to mechanical vibrations induced by the oscillating magnetic field. Kim et al.<sup>41</sup> also used alternating magnetic field of very low frequency (on the order of tens of Hz creating an oscillation), which transmits a mechanical force to the cell causing cell death. Edelman et al.,<sup>42</sup> similarly, advocated mechanical effects in drug release in the presence of an oscillating magnetic field. Most of these studies relating the release behavior and/or cell death to mechano-magnetic effects have been conducted with low-frequency oscillating fields.

The present work demonstrates the potential for the soft polymeric hydrogel nanoconstruct encapsulated with MNS in diagnostic MR imaging as well as inhibiting cancer under high-frequency RF field. The aqueous stabilized MNS embedded into hydrogels; especially MNHG-PEG-12 with 12 nm PEG-functionalized MNS resulted in high value of transverse relaxivity. The composition further exhibited enhanced drug release and cell killing efficacy under externally applied RF field. Quantitatively, 80% cell death occurred because of synergistic

effect of local heating as well as magnetic oscillations when HeLa cell lines incubated with sample exposed to RF field for an hour. Several other recent attempts<sup>43–46</sup> carried out toward this are valuable and extended to the understanding of RF-induced therapeutics release with no emphasis on investigation of cell killing efficacy with anti-cancer agents or uptake of hydrogels, which forms promise for real applications. Some other works in this direction where particular nanocarriers<sup>47,48</sup> loaded with MNS were used to treat cancer cells are noteworthy here; however, reports on hydrogel-based carriers are limited. We believe these results are promising and open up a new modality to diagnose and treat cancer through noninvasive remotely controlled chemotherapeutic using hydrogel nanoconstructs where the therapeutic agent can be delivered because of the synergistic effect of local heat as well as magneto-mechanical oscillation of the soft polymeric segments.

## 5. SUMMARY & CONCLUSIONS

The nanoscale magnetic hydrogels based on poly(*N*-isopropylacrylamide) were developed for theranostic application. The hydrogels embedded with low concentration of Fe<sub>3</sub>O<sub>4</sub> magnetic nanostructures (MNS) resulted in an LCST of ~40 °C. No macroscopic temperature rise was noticeable when magnetic hydrogels were placed in the RF field for up to 1 h, mainly because of a localized rise in temperature in the micro-environmental surrounding of MNS, which dissipates heat rapidly inside hydrogels. The system with PEG-functionalized MNS of the size of 12 nm (HGMNS-PEG-12) was observed to have sufficient MR relaxivity ( $r_2$ ) values (173 mM<sup>-1</sup> s<sup>-1</sup>). The system was further investigated for its efficacy for drug delivery and cytotoxicity using HeLa cell lines. RF-induced drug release experiment showed more than two-fold enhanced release of DOX as compared with room temperature released amount. Further in vitro cell death of approximately 80% was observed under the RF field as compared to only 30% without RF exposure. In conclusion, we believe that the hydrogel system embedded with PEG-functionalized MNS with 12 nm size is an excellent candidate for theranostic applications where therapy and diagnostics are performed using the same agent.

## ■ ASSOCIATED CONTENT

### Supporting Information

XRD, FT-IR, and XPS data for Fe<sub>3</sub>O<sub>4</sub> MNS. NMR spectra for polyNIPAAm hydrogels, iron concentration, and magnetization measurements of HGMNS samples. The experimental protocols and fluorescence spectra evolution results for cargo (fluorescein and DOX) encapsulation and release. Cumulative drug release of DOX from HGMNS-PEG-12. Brief investigation about distorted morphology of hydrogels after cell uptake through STEM. This material is available free of charge via the Internet at <http://pubs.acs.org/>.

## ■ AUTHOR INFORMATION

### Corresponding Authors

\*E-mail: v-dravid@northwestern.edu.  
\*E-mail: dhiren@iitb.ac.in.

### Notes

The authors declare no competing financial interest.

## ■ ACKNOWLEDGMENTS

This research was supported primarily by the Center of Cancer Nanotechnology Excellence (CCNE) initiative of the National

Institutes of Health (NIH) under Award number U54 CA151880. The content is solely the responsibility of the authors and does not necessarily represent the official views of the National Cancer Institute or the National Institutes of Health. Part of this work was performed in EPIC/NIFTI facility of NUANCE center at Northwestern University. Authors are thankful to Dr. Jinsong Wu, Yi-Kai Huang and Dr. Keith Macrenaris for their help and assistance with TEM, SEM, and study the cellular uptake of iron quantification, respectively. The authors acknowledge the help of Akshay K. Swain, IIT Bombay, India, in SQUID magneto-measurements. Prof. D. Bahadur was also supported under the Faculty Mobility Program between IITB and NU McCormick.

## ■ ABBREVIATIONS

Poly(NIPAAm), poly(*N*-isopropylacrylamide)

MNS, magnetic nanostructure

HG, hydrogel

HGMNS, hydrogel-magnetic nanostructure

LCST, lower critical solution temperature

DOX, doxorubicin

PEG, poly-ethylene glycol

POSS, polyhedral oligomeric silsesquioxane

STEM, scanning transmission electron microscopy

DSC, differential scanning calorimetry

HGMNS-PEG-9 and HGMNS-POSS-9, denote the hydrogel-MNS system embedded with MNS of the size 9 nm functionalized by PEG and POSS molecules respectively

## ■ REFERENCES

- (1) Matsumoto, N. M.; Prabhakaran, P.; Rome, L. H.; Maynard, H. D. Smart Vaults: Thermally-Responsive Protein Nanocapsules. *ACS Nano* **2013**, *7*, 867–874.
- (2) Alarcon, C. H.; Pennadam, S.; Alexander, C. Stimuli Responsive Polymers for Biomedical Applications. *Chem. Soc. Rev.* **2005**, *34*, 276–285.
- (3) Kim, D.-H.; Vitol, E. A.; Liu, J.; Balasubramanian, S.; Gosztola, D. J.; Cohen, E. E.; Novosad, V.; Rozhkova, E. A. Stimuli-Responsive Magnetic Nanomicelles as Multifunctional Heat and Cargo Delivery Vehicles. *Langmuir* **2013**, *29*, 7425–7432.
- (4) Sahoo, B.; Devi, K. S. P.; Banerjee, R.; Maiti, T. K.; Pramanik, P.; Dhara, D. Thermal and pH Responsive Polymer-Tethered Multifunctional Magnetic Nanoparticles for Targeted Delivery of Anticancer Drug. *ACS Appl. Mater. Interfaces* **2013**, *5*, 3884–3893.
- (5) De Paoli, M.V.; Lacerda, S. H. D. P.; Spinu, L.; Ingber, B.; Rosenzweig, Z.; Rosenzweig, N. Effect of an Oscillating Magnetic Field on the Release Properties of Magnetic Collagen Gels. *Langmuir* **2006**, *22*, 5894–5899.
- (6) Hu, S.-H.; Liao, B.-J.; Chiang, C.-S.; Chen, P.-J.; Chen, I.-W.; Chen, S.-Y. Core-Shell Nanocapsules Stabilized by Single-Component Polymer and Nanoparticles for Magneto-Chemotherapy/Hyperthermia with Multiple Drugs. *Adv. Mater.* **2012**, *24*, 3627–3632.
- (7) Chiang, W.-L.; K, C.-J.; Liao, Z.-X.; Chen, S.-Y.; Chen, F.-R.; Tsai, C.-Y.; Xia, Y.; Sung, H.-W. Pulsatile Drug Release from PLGA Hollow Microspheres by Controlling the Permeability of Their Walls with a Magnetic Field. *Small* **2012**, *8* (23), 3584–3588.
- (8) Peiris, P. M.; Bauer, Lisa.; Toy, R.; Tran, E.; Pansky, J.; Doolittle, E.; Schmidt, E.; Hayden, E.; Mayer, A.; Keri, R.; Griswold, M. A.; Karathanasis, E. Enhanced Delivery of Chemotherapy to Tumors Using a Multicomponent Nanochain with Radio-Frequency-Tunable Drug Release. *ACS Nano* **2012**, *6*, 4157–4168.
- (9) De, M.; Chou, S. S.; Joshi, H.; Dravid, V. P. Hybrid Magnetic Nanostructures (MNS) for Magnetic Resonance Imaging Applications. *Adv. Drug Delivery Rev.* **2011**, *63*, 1282–1299.
- (10) Rubio-Retama, J.; Zafeiropoulos, N. E.; Serafinelli, C.; Rojas-Reyna, R.; Voit, B.; Cabarcos, E. L.; Stamm, M. Synthesis and

- Characterization of Thermosensitive PNIPAM Microgels Covered with Superparamagnetic  $\gamma$ -Fe<sub>2</sub>O<sub>3</sub> Nanoparticles. *Langmuir* **2007**, *23*, 10280–10285.
- (11) Jaiswal, M. K.; Banerjee, R.; Pradhan, P.; Bahadur, D. Thermal Behavior of Magnetically Modalized Poly(N-Isopropylacrylamide)-Chitosan based Nanohydrogel. *Colloid Surf. B* **2010**, *81*, 185–194.
- (12) Jaiswal, M. K.; Mehta, S.; Banerjee, R.; Bahadur, D. A Comparative Study on Thermoresponsive Magnetic Nanohydrogels: Role of Surface-Engineered Magnetic Nanoparticles. *Colloid. Polym. Sci.* **2012**, *290*, 607–617.
- (13) Han, H. D.; Shin, B. C.; Choi, H. S. Doxorubicin-Encapsulated Thermosensitive Liposomes Modified with Poly(N-isopropylacrylamide-co-acrylamide): Drug Release Behaviour and Stability in the Presence of Serum. *Eur. J. Pharma. Biopharma.* **2006**, *62*, 110–116.
- (14) Lo, C.-L.; Lin, K.-M.; Hsieh, G.-H. Preparation and Characterization of Intelligent Core-Shell Nanoparticles based on Poly(d,l-lactide)-g-Poly(N-isopropylacrylamide-co-Methacrylic acid). *J. Controlled Release* **2005**, *104*, 477–488.
- (15) Li, Z.; Shen, J.; Ma, H.; Lu, X.; Shi, M.; Li, N.; Ye, M. Preparation and Characterization of Sodium Alginate/Poly(N-isopropylacrylamide)/Clay Semi-IPN Magnetic Hydrogels. *Polym. Bull.* **2012**, *68*, 1153–1169.
- (16) Baeza, A.; Guisasola, E.; Ruiz-Hernández, E.; Vallet-Regí, M. Magnetically Triggered Multidrug Release by Hybrid Mesoporous Silica Nanoparticles. *Chem. Mater.* **2012**, *24*, 517–524.
- (17) Sivakumaran, D.; Maitland, D.; Hoare, T. Injectable Microgel-Hydrogel Composites for Prolonged Small-Molecule Drug Delivery. *Biomacromolecules* **2011**, *12*, 4112–4120.
- (18) Tan, H.; Ramirez, C. M.; Miljkovic, N.; Li, H.; Rubin, J.P.; Marra, K.G. Thermosensitive Injectable Hyaluronic Acid Hydrogel for Adipose Tissue Engineering. *Biomaterials* **2009**, *30*, 6844–6853.
- (19) Yang, J.; Yamato, M.; Shimizu, T.; Sekine, H.; Ohashi, K.; Kanzaki, M.; Ohki, T.; Nishida, K.; Okano, T. Reconstruction of Functional Tissues with Cell Sheet Engineering. *Biomaterials* **2007**, *28*, 5033–5043.
- (20) Hong, S. W.; Kim, D. Y.; Lee, J. U.; Jo, W. H. Synthesis of Polymeric Temperature Sensor Based on Photophysical Property of Fullerene and Thermal Sensitivity of Poly(N-Isopropylacrylamide). *Macromolecules* **2009**, *42*, 2756–2761.
- (21) Yang, C. C.; Tian, Y.; Jen, A. K.-Y.; Chen, W.-C. J. New Environmentally Responsive Fluorescent N-isopropylacrylamide Copolymer and Its Application to DNA Sensing. *Polym. Sci. A* **2006**, *44*, 5495–5504.
- (22) Parasuraman, D.; Serpe, M. J. Poly (N-Isopropylacrylamide) Microgels for Organic Dye Removal from Water. *ACS Appl. Mater. Interfaces* **2011**, *3*, 4714–4721.
- (23) Kubo, S.; Tan, I.; White, R. J.; Antonietti, M.; Titirici, M. M. Template Synthesis of Carbonaceous Tubular Nanostructures with Tunable Surface Properties. *Chem. Mater.* **2010**, *22*, 6590–6597.
- (24) Amstad, E.; Gillich, T.; Bilecka, I.; Textor, M.; Reimhult, E. Ultrastable Iron Oxide Nanoparticle Colloidal Suspensions Using Dispersants with Catechol-Derived Anchor Groups. *Nano Lett.* **2009**, *9*, 4042–4048.
- (25) Frankamp, B. L.; Fischer, N. O.; Hong, R.; Srivastava, S.; Vincent M. Rotello, V. M. Surface Modification Using Cubic Silsesquioxane Ligands. Facile Synthesis of Water-Soluble Metal Oxide Nanoparticles. *Chem. Mater.* **2006**, *18*, 956–959.
- (26) Kumagai, M.; Sarma, T. K.; Cabral, H.; Kaida, S.; Sekino, M.; Herlambang, N.; Osada, K.; Kano, M. R.; Nishiyama, N.; Kataoka, K. Enhanced In vivo Magnetic Resonance Imaging of Tumors by PEGylated Iron-Oxide–Gold Core–Shell Nanoparticles with Prolonged Blood Circulation Properties. *Macromol. Rapid Commun.* **2010**, *31*, 1521–1528.
- (27) Sun, C.; Du, K.; Fang, C.; Bhattacharai, N.; Veiseh, O.; Kievit, F.; Stephen, Z.; Lee, D.; Ellenbogen, R. G.; Ratner, B.; Zhang, M. PEG-Mediated Synthesis of Highly Dispersive Multifunctional Superparamagnetic Nanoparticles: Their Physicochemical Properties and Function In Vivo. *ACS Nano* **2010**, *4*, 2402–2410.
- (28) Park, J.; An, K.; Hwang, Y.; Park, J.-G.; Noh, H.-J.; Kim, J.-Y.; Park, J.-H.; Hwang, N.-M.; Hyeo, T. Biofunctionalized Magnetic-Vortex Microdisks for Targeted Cancer-Cell Destruction. *Nat. Mater.* **2004**, *3*, 891–895.
- (29) Oliveira, H.; P.-Andrés, E.; Thevenot, J.; Sandre, O.; Berra, E.; LeCOMMANDOUX, S. Magnetic Field Triggered Drug Release from Polymersomes for Cancer Therapeutics. *J. Controlled Release* **2013**, *169*, 165–170.
- (30) Goiti, E.; Salinas, M. M.; Arias, G.; Puglia, D.; Kenny, J. M.; Mijangos, C. ABS/Clay Nanocomposites Obtained by a Solution Technique: Influence of Clay Organic Modifiers. *Polym. Degrad. Stab.* **2007**, *92*, 2198–2205.
- (31) Kobayashi, M.; Rharbi, Y.; Brauge, L.; Cao, L.; Winnik, M. A. Effect of Silica as Fillers on Polymer Interdiffusion in Poly(butyl methacrylate) Latex Films. *Macromolecules* **2002**, *35*, 7387–7399.
- (32) Hu, F.; Joshi, H. M.; Dravid, V. P.; Meade, T. J. High-Performance Nanostructured MR Contrast Probes. *Nanoscale* **2010**, *2*, 1884–1891.
- (33) Vuong, Q. L.; Berret, J.-F.; Fresnais, J.; Gossuin, Y.; Sandre, O. A Universal Scaling Law to Predict the Efficiency of Magnetic Nanoparticles as MRI T2-Contrast Agents. *Adv. Healthcare Mater.* **2012**, *1*, 502–512.
- (34) Pothayee, N.; Balasubramaniam, S.; Pothayee, N.; Jain, N.; Hu, N.; Lin, Y.; Davis, R. M.; Sriranganathan, N.; Koretsky, A. P.; Riffle, S. Magnetic Nanoclusters with Hydrophilic Spacing for Dual drug Delivery and Sensitive Magnetic Resonance Imaging. *J. Mater. Chem. B* **2013**, *1*, 1142–1149.
- (35) Barick, K. C.; Aslam, M.; Lin, Y.-P.; Bahadur, D.; Prasad, P. V.; Dravid, V. P. Novel and Efficient MR Active Aqueous Colloidal Fe<sub>3</sub>O<sub>4</sub> Nanoassemblies. *J. Mater. Chem.* **2009**, *19*, 7023–7029.
- (36) Balasubramaniam, S.; Pothayee, N.; Lin, Y.; House, M.; Woodward, R. C.; St. Pierre, T. G.; Davis, R. M.; Riffle, J. S. Poly(N-isopropylacrylamide)-Coated Superparamagnetic Iron Oxide Nanoparticles: Relaxometric and Fluorescence Behavior Correlate to Temperature-Dependent Aggregation. *Chem. Mater.* **2011**, *23*, 3348–3356.
- (37) H. Zhu, H.; J. Tao, J.; W. Wang, W.; Y. Zhou, Y.; P. Li, P.; Z. Li, Z.; K. Yan, K.; S. Wu, S.; Yeung, K. W. K.; Xu, Z.; Xu, H.; Chu, P. K. Magnetic, Fluorescent, and Thermo-responsive Fe<sub>3</sub>O<sub>4</sub>/Rare Earth Incorporated Poly(St-NIPAM) Core–Shell Colloidal Nanoparticles in Multimodal Optical/Magnetic Resonance Imaging Probes. *Biomaterials* **2013**, *34*, 2296–2306.
- (38) Polo-Corrales, L.; Rinaldi, C. Monitoring Iron Oxide Nanoparticle Surface Temperature in an Alternating Magnetic Field using Thermoresponsive Fluorescent Polymers. *J. Appl. Phys.* **2012**, *111*, 07B334.
- (39) Asin, L.; Goya, G.F.; Tres, A.; Ibarra, M.R. Induced Cell Toxicity Originates Dendritic Cell Death Following Magnetic Hyperthermia Treatment. *Cell Death Dis.* **2013**, *4*, e596.
- (40) Brûlé, S.; Levy, M.; Wilhelm, C.; Letourneur, D.; Gazeau, F.; Ménager, C.; Le Visage, C. Doxorubicin Release Triggered by Alginate Embedded Magnetic Nanoheaters: A Combined Therapy. *Adv. Mater.* **2011**, *23*, 787–790.
- (41) Kim, D.-H.; Rozhkova, E. A.; Ulasov, I. V.; Bader, S. D.; Rajh, T.; Lesniak, M. S.; Novosad, V. Biofunctionalized Magnetic-Vortex Microdisks for Targeted Cancer-Cell Destruction. *Nat. Mater.* **2010**, *9*, 165–171.
- (42) Edelman, E.R.; Langer, R. Optimization of Release from Magnetically Controlled Polymeric Drug Release Devices. *Biomaterials* **1993**, *14*, 621–626.
- (43) Campbell, S. B.; Patenaude, M.; Hoare, T. Injectable Superparamagnets: Highly Elastic and Degradable Poly(N-isopropylacrylamide)–Superparamagnetic Iron Oxide Nanoparticle (SPION) Composite Hydrogels. *Biomacromolecules* **2013**, *14*, 644–653.
- (44) Satarkar, N. S.; Hilt, J. Z. Magnetic Hydrogel Nanocomposites for Remote Controlled Pulsatile Drug Release. *J. Controlled Release* **2008**, *130*, 246–251.
- (45) Deng, Y.; Wang, C.; Shen, X.; Yang, W.; Jin, L.; Gao, H.; Fu, S. Preparation, Characterization, and Application of Multistimuli-

Responsive Microspheres with Fluorescence-Labeled Magnetic Cores and Thermoresponsive Shells. *Chem.—Eur. J.* **2005**, *11*, 6006–6013.

(46) Serpe, M. J.; Yarmey, K. A.; Nolan, C. M.; Lyon, A. Doxorubicin Uptake and Release from Microgel Thin Films. *Biomacromolecules* **2005**, *6*, 408–413.

(47) Sanson, C.; Odile, D.; Julie, T.; Emmanuel, I.; Alain, S.; Annie, B.; Sylvain, M.; Eric, T.; Sisareuth, T.; Alain, B.; Vincent, D.; Sandre, O.; Sébastien, L. Doxorubicin Loaded Magnetic Polymersomes: Theranostic Nanocarriers for MR Imaging and Magneto-Chemotherapy. *ACS Nano* **2011**, *5*, 1122–1140.

(48) Plassat, V.; Wilhelm, C.; Marsaud, V.; Ménager, C.; Gazeau, F.; Renoir, J.-M.; Lesieur, S. Anti-Estrogen-Loaded Superparamagnetic Liposomes for Intracellular Magnetic Targeting and Treatment of Breast Cancer Tumors. *Adv. Funct. Mater.* **2011**, *21*, 83–92.